Experimental study of shock wave modulation caused by velocity and temperature fluctuations in cylinder wakes

Kento Inokuma,[1,*] Tomoaki Watanabe,[2] Koji Nagata,[2] and Yasuhiko Sakai[3]
[1]*Department of Mechanical Systems Engineering, Tokyo University of Agriculture and Technology, Tokyo 184-8588, Japan*
[2]*Department of Aerospace Engineering, Nagoya University, Nagoya 464-8603, Japan*
[3]*Institute of International Education and Exchange, Nagoya University, Nagoya 464-8601, Japan*

(Received 24 December 2020; accepted 1 June 2021; published 14 June 2021)

Experiments on a spherical shock wave propagating across an unheated- or a heated-cylinder wake are performed in a wind tunnel to investigate the effects of velocity and temperature fluctuations of turbulence on the shock wave. The temperature of the heated cylinder is low enough for the buoyancy effect to be negligible in the wake development, and comparisons between the heated- and unheated-cylinder experiments highlight the effects of temperature fluctuations on the shock wave. Peak overpressure of the spherical shock wave is measured on a wall after the shock wave has passed the wake. Along with the overpressure measurement, temperature and velocity are measured in the heated and unheated wakes, respectively. Larger peak-overpressure fluctuations are obtained when the shock wave interacts with the heated-cylinder wake than with the unheated-cylinder wake. Correlation coefficients are calculated between the velocity/temperature fluctuations of the unheated/heated-cylinder wakes and peak-overpressure fluctuations. The temperature fluctuations and overpressure fluctuations are found to be negatively correlated, which is explained by the shock deformation caused by speed-of-sound fluctuations in front of the shock wave. By comparing the correlation coefficients between velocity and overpressure fluctuations with those between temperature and overpressure fluctuations, it is also discovered that the temperature fluctuations of the heated-cylinder wake have a stronger correlation with the overpressure fluctuations than the velocity fluctuations of the unheated-cylinder wake.

DOI: 10.1103/PhysRevFluids.6.063401

I. INTRODUCTION

Shock wave propagation in turbulent flows causes the shock-turbulence interaction, which is widely seen in science and engineering problems. It can be observed, for example, in the galaxy formations caused by a supernova explosion [1]. In nuclear physics, the duration time of confinement fusion is affected by the turbulence characteristics interacting with the shock wave [2]. It is also important in engineering applications, such as in the sonic boom problem caused by supersonic flight. The pressure waveforms of a sonic boom are known to be significantly modulated in the atmospheric turbulence [3]. Another important engineering problem of the shock-turbulence interaction is the shock–boundary-layer interaction, which occurs in air intakes of supersonic jet engines and on transonic airfoils of aeronautics, causing a decline in the aerodynamic flight performance [4–7]. For the further understanding of such phenomena and improvement of related engineering

*inokuma@go.tuat.ac.jp

equipment, it is crucial to investigate the shock-turbulence interaction from the fundamental aspects of the problems.

There have been some laboratory-scale studies of the shock-turbulence interaction. Inner shock tube experiments [8,9] and wind tunnel experiments [10] reported changes in turbulence characteristics after the interaction, such as amplifications of velocity fluctuations [9,10], vorticity fluctuations [9], and density fluctuations [8]. The shock-turbulence interaction also causes changes in shock wave characteristics. An increase in the shock wave overpressure fluctuations after the interaction was observed in experiments of shock waves propagating in grid turbulence [11,12] and jets [13,14]. The geometrical properties of a planar shock wave interacting with grid turbulence were visualized in inner shock tube experiments [15], where the shock wave surface was largely deformed after the interaction with turbulence. Numerical and theoretical studies have also been performed in order to investigate the effects of the interaction on the characteristics of shock waves and turbulence [16–23]. One of the important results of those studies is the discovery of the broken shock wave regime, which is the local disappearance of the shock wave surface caused by turbulence [16,17,19,20].

There have been several attempts to systematically assess the shock-turbulence interaction by representing the statistics of the shock wave and turbulence after the interaction as functions of a few parameters of the problems. Most previous studies considered the shock Mach number, turbulent Mach number, and turbulent Reynolds number as dominant parameters of the shock-turbulence interaction [16–18,20]. The shock Mach number represents the intensity of the shock wave. The turbulent Mach number is defined with the ratio between root-mean-squared (rms) velocity fluctuations and mean speed of sound, and it can be considered as the intensity of turbulent velocity fluctuations. The turbulent Reynolds number is one of the parameters that has been used to represent the ratio of length scales of turbulence and shock width [18,19]. One might immediately notice that none of these parameters is directly associated with fluctuations of thermodynamic properties of a fluid in which the shock wave propagates. Once temperature fluctuations are induced in turbulent flows, they can significantly affect the shock wave propagation because the local speed of sound depends on temperature. In compressible turbulence, the turbulent Mach number implicitly takes temperature fluctuations into account as strong compressibility that causes non-negligible temperature fluctuations by viscous heating and dilatational effects in turbulence [16]. However, it is important to treat fluctuations of thermodynamic characteristics separately from velocity fluctuations because temperature fluctuations can also be introduced in a flow without strong compressibility, such as a plume of heated air. Previous numerical studies have investigated the thermodynamic characteristics of turbulence, such as fluctuations in temperature, entropy, and acoustic pressure after interacting with a shock wave [24–28], in which compressible turbulence has been decomposed into vortical, entropic, and acoustic modes by using Kovasznay's modal decomposition [29]. However, these studies have not focused on the change in the shock wave characteristics, and the role of the thermodynamic characteristics of turbulence in the shock wave modulation is not clear. In previous experimental work, pressure waveforms of a shock wave interacting with thermal turbulence were measured, where the statistics of the peak overpressure behind the shock wave were obtained [30]. However, in their study, the effects of temperature fluctuations could not be evaluated separately from those of the vertical convection caused by buoyancy of the thermal turbulence. Moreover, an investigation of the role of temperature fluctuations requires simultaneous measurements of both temperature in turbulence and shock wave overpressure in order to obtain the relation between temperature and overpressure fluctuations. However, such measurements have not been conducted in previous studies.

The purpose of this study is to experimentally reveal the effects of temperature fluctuations in turbulence on the shock wave. We obtain statistical data of the shock wave characteristics in experiments on a spherical shock wave propagating in a heated-cylinder wake or an unheated-cylinder wake, where a comparison between the heated and unheated cases highlights the effects of temperature fluctuation on the shock wave. Low temperature is considered for the heated cylinder so that the buoyancy effect of the heated cylinder wake can be ignored. Measurements are conducted

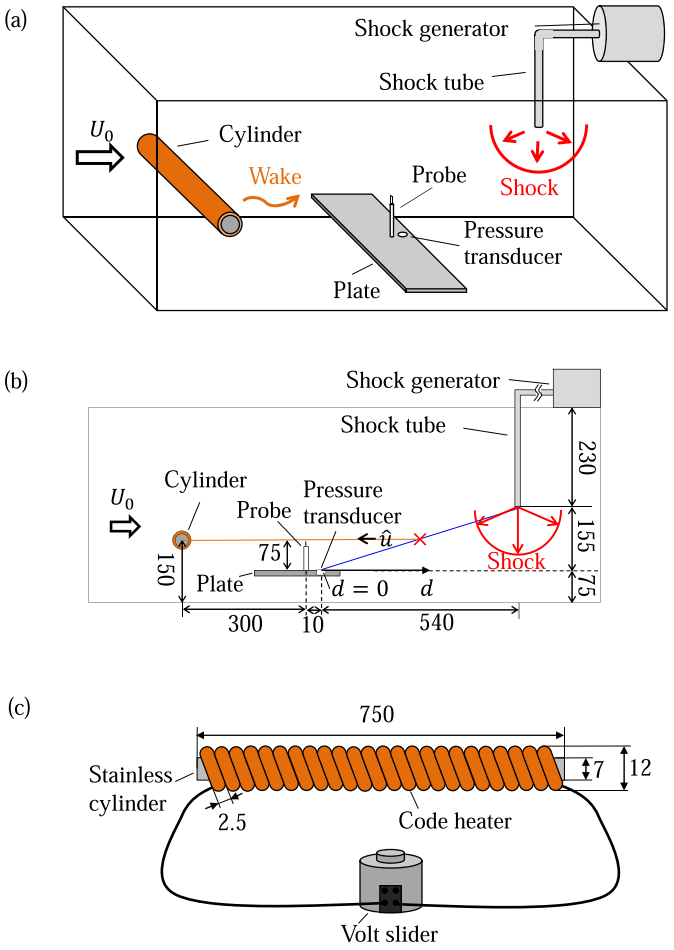

FIG. 1. (a) Schematic of the experimental setup. (b) Side view of the test section. Orange and blue lines show the centerline of the cylinder wake and shock ray from the shock tube end to the pressure transducer, respectively. The red cross shows the intersection of the wake centerline and the shock ray. The distance between the cylinder center and the red cross is 561 mm. (c) Schematic of the heater-wrapped cylinder. Lengths are shown in mm.

for temperature and velocity in the wakes and overpressure behind the shock wave on a wall. Statistical analysis and discussion based on shock surface deformation clarify how the temperature fluctuations in turbulence affect the shock wave characteristics.

II. EXPERIMENTS OF INTERACTION BETWEEN SPHERICAL SHOCK WAVE AND TURBULENT CYLINDER WAKES

A. Experimental setup and conditions

Figures 1(a) and 1(b) outline the experiments of a spherical shock wave that propagates in the heated- or unheated-cylinder wake, where the wind tunnel and shock wave generator used in this study are the same as those in our previous studies [11,12,31–33]. A silicon code heater (diameter: 2.5 mm) is wrapped around a stainless cylinder (diameter: 7 mm). The total diameter of the cylinder with the heater is $D = 12$ mm, as shown in Fig. 1(c). The cylinder is horizontally placed in the

TABLE I. Experimental conditions. $\mathrm{Re}_D = U_0 D/\nu$ is the Reynolds number based on the cylinder diameter (ν is the kinematic viscosity). The rms streamwise velocity fluctuation u_{rms}, velocity defect ΔU, Taylor microscale λ, longitudinal velocity integral length scale L_u, half-width based on ΔU, b_U, temperature increase ΔT, the rms temperature fluctuation T_{rms}, longitudinal temperature integral length scale L_T, and half-width based on ΔT, b_T in the table are measured at 561 mm ($\approx 47D$) downstream from the cylinder center [at the point of the red cross in Fig. 1(b)]. M_{S0} is the shock Mach number at the pressure transducer location.

Case	1-OFF	2-OFF	3-OFF	1-ON	2-ON	3-ON
Symbol	△ (blue)	□ (blue)	◯ (blue)	△ (red)	□ (red)	◯ (red)
U_0 (m/s)	2.5	5	10	2.5	5	10
Re_D	2100	4200	8400	2100	4200	8400
ΔU (m/s)	0.427	0.980	1.75	0.427	0.980	1.75
u_{rms} (m/s)	0.204	0.361	0.749	0.204	0.361	0.749
λ (mm)	3.42	3.24	4.45	3.42	3.24	4.45
L_u (mm)	19.4	24.5	59.4	19.4	24.5	59.4
b_U (mm)	28.4	28.0	29.9	28.4	28.0	29.9
ΔT (K)				1.51	1.22	0.998
Ri				1.35×10^{-2}	3.38×10^{-3}	8.44×10^{-4}
T_{rms} (K)				0.305	0.186	0.128
L_T (mm)				67.0	36.1	28.0
b_T (mm)				49.4	57.0	87.8
M_{S0}	1.004	1.004	1.004	1.004	1.004	1.004

wind tunnel. The heated cylinder experiments are conducted by applying a voltage of 130 V to the heater with a volt slider (Yamabishi Electric Co., LTD. V-130-5) while the volt slider is turned off in the experiments of the unheated cylinder wake. The turbulent wake with velocity and temperature fluctuations is formed behind the heated cylinder [34–36]. Shock waves are produced with the shock wave generator, in which a driver gas (air at 900 kPa) is separated from a driven gas (air at ambient pressure) with a quick piston valve. After the shock wave is ejected from the open end of the shock tube, it spherically propagates in the turbulent cylinder wake in the test section.

We consider six experimental conditions of the cylinder wakes as shown in Table I, which are realized by changing the mean streamwise velocity U_0 set in the wind tunnel and heater conditions (OFF/ON). The Reynolds number based on the cylinder diameter D, $\mathrm{Re}_D = U_0 D/\nu$ (ν is the kinematic viscosity), ranges from 2100 to 8400. The velocity defect and temperature increase are defined with $\Delta U = U_0 - U_{\mathrm{ave}}$ and $\Delta T = T_{\mathrm{ave}} - T_0$, respectively, where U_{ave} and T_{ave} are the time-averaged velocity and temperature, and T_0 is the room temperature. The experiments are conducted for unheated-cylinder wakes (heater: OFF) and heated-cylinder wakes (heater: ON). The velocity ranges between 2.5 and 10 m/s. In cases 1-OFF, 2-OFF, and 3-OFF, the heater is turned off, and the spherical shock wave interacts with the unheated-cylinder wake, where no temperature fluctuations are induced by the cylinder. The effects of the turbulent wake on the shock wave are attributed solely to the velocity field of the wake. On the other hand. the heater is turned on in cases 1-ON, 2-ON, and 3-ON, where the heated-cylinder wake is formed in the test section. Both temperature and velocity in the wake affect the shock wave characteristics. Temperature measurements in the heated wake in the next section show that with the present conditions, the temperature difference between the wake and freestream is small enough for the buoyancy effects to be negligible in the wake development. Therefore, the contribution of the temperature distribution in the wake is evaluated via a comparison between the heated- and unheated-cylinder experiments with the same U_0.

Buoyancy effects in the heated-cylinder wake can be assessed by the Richardson number $\mathrm{Ri} = g\beta(T_{\mathrm{W}} - T_0)D/{U_0}^2$, where g is the gravitational acceleration, β is the bulk modulus, and T_{W} is the mean temperature on the cylinder surface. When $U_0 = 0$ m/s, T_{W} measured with a thermocouple is 220 °C. T_{W} at $U_0 = 0$ m/s is used for the calculations of Ri summarized in Table I. The actual

R_i can be smaller since T_W becomes smaller when $U_0 > 0$ as in our experiments. When Ri < 0.5, the buoyancy effect can be ignored in the flow characteristics compared to the forced convection effect [37–40]. Since Ri considered in our study is Ri $\ll 0.5$, the buoyancy effect is small and can be assumed not to influence the velocity characteristics.

B. Measurement methods

A measurement plate is installed in the test section, which is equipped with a pressure transducer (PCB Piezotronics Inc. 113B27) and a probe. Here, we use DANTEC StreamLine for velocity and temperature measurements with an I-type hot-wire probe (DANTEC DYNAMICS 55P11) and a cold-wire probe (DANTEC DYNAMICS 55P11), respectively. The pressure transducer measures overpressure on the plate, where the overpressure rise is observed upon the arrival of the shock wave. The hot-wire and cold-wire probes are used for measuring velocity and temperature on the wake centerline. Here, the hot-wire probe is used in the unheated-cylinder experiments while the cold-wire probe is used in the heated-cylinder experiments. Therefore, the overpressure on the wall is simultaneously measured with velocity and temperature in the wake in the unheated- and heated-cylinder experiments, respectively. The ejection of the shock wave and the signal sampling are controlled by a computer and a scope coder (YOKOGAWA, DL850E). The signal sampling frequency of the scope coder is 1 MHz. For each experimental case, we repeat the shock wave ejections 400 times for the statistical analyses discussed below. The shock Mach numbers M_{S0} in Table I are estimated from the ensemble averages of the peak overpressure measured at the pressure transducer location as in our previous studies [11,12].

III. SHOCK DEFORMATION MODEL FOR SHOCK PROPAGATION IN A FLOW WITH VELOCITY AND TEMPERATURE FLUCTUATIONS

In our previous study, the shock deformation model was used for weak shock wave propagation in a velocity fluctuating field [12]. In the model, the surface deformation of the shock wave which propagates in a local cylindrical turbulent region with a streamwise length of x_l and a radius of r_0 was estimated by considering the local movement velocity of the shock wave as shown in Fig. 2. The small shock deformation was considered, where the deformation was assumed to be a linear inclination of the shock wave surface. The change in the shock Mach number of the deformed shock wave was obtained from the change in the cross-sectional area of the ray tube of the shock wave by using Whitham's ray-shock theory [41]. In this study, we extend the model to the shock propagation in the velocity and temperature fluctuating field. As shown in Fig. 2, axisymmetric profiles of velocity $u_M(x, r)$ and temperature $T_M(x, r)$ are given at time $t = 0$ in front of the shock wave, where x and r are the axial and radial coordinates, respectively. Here, u_M is given as

$$u_M(x, r) = \begin{cases} u & (0 \leqslant r \leqslant r_0 \text{ and } 0 \leqslant x \leqslant x_l), \\ 0 & \text{otherwise}, \end{cases} \tag{1}$$

which is the same as in the previous model (see Ref. [12]).

T_M is given as

$$T_M(x, r) = \begin{cases} T_0 + T' & (0 \leqslant r \leqslant r_0 \text{ and } 0 \leqslant x \leqslant x_l), \\ T_0 & \text{otherwise} \end{cases} \tag{2}$$

with uniform temperature T_0 and a fluctuating component T'. Here, u and T' are assumed to be stochastic variables, and in the model, one realization of a flow field for a set of u and T' is considered. The movement velocity of the shock wave in the velocity and temperature fluctuating region ($r \leqslant r_0$) is

$$V_S = aM_S + u, \tag{3}$$

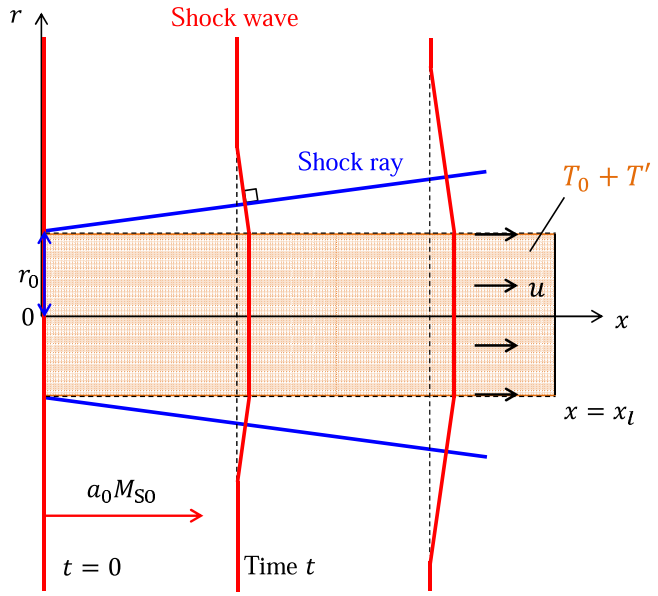

FIG. 2. Schematic of shock wave deformation due to local velocity fluctuation u and temperature fluctuation T'. The orange area shows $0 \leqslant r \leqslant r_0$ and $0 \leqslant x \leqslant x_l$, where $u_M = u$ and $T_M = T_0 + T'$ at $t = 0$.

where $a = \sqrt{\gamma R(T_0 + T')}$, γ is the heat capacity ratio, R is the gas constant, and M_S is the shock Mach number. Then, the difference of the movement velocity of the shock wave between $r \leqslant r_0$ and $r > r_0$, $V'_S = V_S - a_0 M_{S0}$ (M_{S0} is the shock Mach number at $x = 0$) is

$$V'_S = a_0 M'_S + M_{S0} a' + a' M'_S + u, \tag{4}$$

where $a_0 = \sqrt{\gamma R T_0}$ is the sound speed at a temperature of T_0, $M'_S = M_S - M_{S0}$ is a fluctuation of the shock Mach number, and $a' = a - a_0$ is a fluctuation of the speed of sound. Since a small shock modulation, $M'_S \ll 1$, is assumed in this model, $a' M'_S$ can be ignored in Eq. (4), and Eq. (4) can be approximated as

$$V'_S \approx a_0 M'_S + M_{S0} a' + u. \tag{5}$$

Thus, as shown in Fig. 2, the shock wave surface is deformed by the movement velocity difference V'_S as it propagates. Compared to the previous model, the effect of the temperature fluctuation T' is considered in the second term on the right-hand side of Eq. (5) as a'. We let Δp be the peak overpressure behind the shock wave, and $\Delta p' = \Delta p - \langle \Delta p \rangle$ be the peak-overpressure fluctuation, where $\langle \Delta p \rangle = 2\gamma p_0 (M_{S0}^2 - 1)/(\gamma + 1)$ (p_0 is the mean pressure in front of the shock wave). In the previous shock deformation model without a sound speed fluctuation [12], $V'_S = a_0 M'_S + u$ was used to calculate the inclination angle of the deformed shock wave, from which M'_S and $\Delta p'$ were obtained by using the Whitham's ray-shock theory [41]. Here, we calculate $\Delta p'$ in a similar manner to that of the previous model but with Eq. (5) instead of $V'_S = a_0 M'_S + u$ as

$$\frac{\Delta p'}{\langle \Delta p \rangle} \approx -\frac{(u + a')/a_0}{\sqrt{M_{S0}^2 - 1}}. \tag{6}$$

The Taylor expansion of a yields

$$a = \sqrt{\gamma R T_0}\left[1 + \frac{T'}{2T_0} + O\left(\frac{T'^2}{T_0^2}\right)\right] = a_0\left[1 + \frac{T'}{2T_0} + O\left(\frac{T'^2}{T_0^2}\right)\right]. \tag{7}$$

Since $T'/T_0 \ll 1$ in our experiments, a'/a_0 can be obtained from Eq. (7) as a function of the first order of T'/T_0 as

$$\frac{a'}{a_0} \approx \frac{T'}{2T_0}, \tag{8}$$

which is substituted into Eq. (6) to obtain

$$\frac{\Delta p'}{\langle \Delta p \rangle} \approx -\frac{u/a_0 + T'/2T_0}{\sqrt{M_{S0}^2 - 1}}. \tag{9}$$

While u, T', and $\Delta p'$ are stochastic variables, the other quantities in Eq. (9), such as $\langle \Delta p \rangle$, a_0, T_0, and M_{S0}, are constants. Then, the calculation of the standard deviations of both sides of Eq. (9) yields

$$\frac{\sigma_{\Delta p}}{\langle \Delta p \rangle} \approx \sqrt{\frac{u_{\rm rms}^2}{a_0^2} + \frac{T_{\rm rms}^2}{4T_0^2} + \frac{\langle uT' \rangle}{a_0 T_0}} \Big/ \sqrt{M_{S0}^2 - 1}, \tag{10}$$

where $\sigma_{\Delta p}$ is the standard deviation of $\Delta p'$, and $u_{\rm rms}$ and $T_{\rm rms}$ are the rms values of u and T'. Here, we define the correlation coefficient between u and T' as $C_{uT} = \langle uT' \rangle / u_{\rm rms} T_{\rm rms}$, which has a value between -1 and 1. Equation (10) can be rewritten as

$$\frac{\sigma_{\Delta p}}{\langle \Delta p \rangle} \approx \sqrt{\frac{u_{\rm rms}^2}{a_0^2} + \frac{T_{\rm rms}^2}{4T_0^2} + C_{uT} \frac{u_{\rm rms} T_{\rm rms}}{a_0 T_0}} \Big/ \sqrt{M_{S0}^2 - 1}. \tag{11}$$

To simplify the notation of Eq. (11), we introduce a function $f(u_{\rm rms}/a_0, T_{\rm rms}/2T_0, C_{uT})$, which is defined as

$$f(u_{\rm rms}/a_0, T_{\rm rms}/2T_0, C_{uT}) = \sqrt{\frac{u_{\rm rms}^2}{a_0^2} + \frac{T_{\rm rms}^2}{4T_0^2} + C_{uT} \frac{u_{\rm rms} T_{\rm rms}}{a_0 T_0}}. \tag{12}$$

Then, Eq. (11) is expressed as follows:

$$\frac{\sigma_{\Delta p}}{\langle \Delta p \rangle} \approx \frac{f(u_{\rm rms}/a_0, T_{\rm rms}/2T_0, C_{uT})}{\sqrt{M_{S0}^2 - 1}}. \tag{13}$$

When temperature is uniform in a flow ($T' = 0$), Eq. (10) becomes

$$\frac{\sigma_{\Delta p}}{\langle \Delta p \rangle} \approx \frac{f(u_{\rm rms}/a_0, 0, 0)}{\sqrt{M_{S0}^2 - 1}} = \frac{u_{\rm rms}/a_0}{\sqrt{M_{S0}^2 - 1}}. \tag{14}$$

The correlation C_{uT} depends on how temperature fluctuations are introduced in a flow. When u/a_0 and $T'/2T_0$ have no correlation, that is, $C_{uT} = 0$, Eq. (10) becomes

$$\frac{\sigma_{\Delta p}}{\langle \Delta p \rangle} \approx \frac{f(u_{\rm rms}/a_0, T_{\rm rms}/2T_0, 0)}{\sqrt{M_{S0}^2 - 1}} = \frac{\sqrt{u_{\rm rms}^2/a_0^2 + T_{\rm rms}^2/4T_0^2}}{\sqrt{M_{S0}^2 - 1}}. \tag{15}$$

When u/a_0 completely coincides with $T'/2T_0$, that is, $C_{uT} = 1$, Eq. (10) becomes

$$\frac{\sigma_{\Delta p}}{\langle \Delta p \rangle} \approx \frac{f(u_{\rm rms}/a_0, T_{\rm rms}/2T_0, 1)}{\sqrt{M_{S0}^2 - 1}} = \frac{u_{\rm rms}/a_0 + T_{\rm rms}/2T_0}{\sqrt{M_{S0}^2 - 1}}. \tag{16}$$

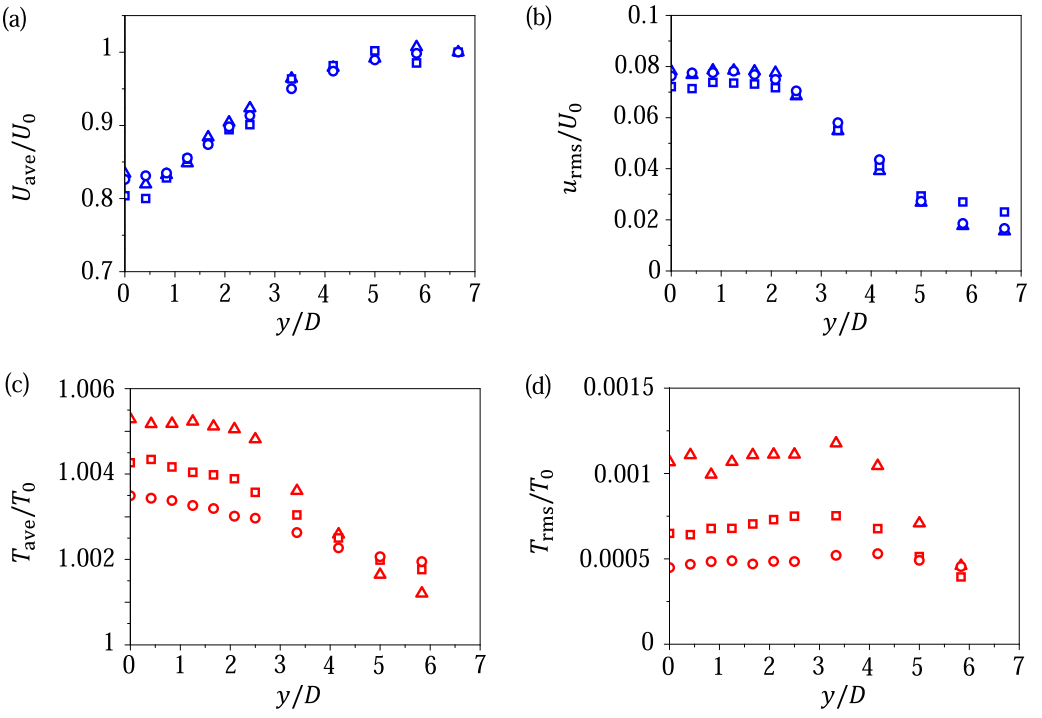

FIG. 3. (a) Time-averaged velocity U_{ave}/U_0 and (b) rms velocity fluctuation u_{rms}/U_0 of the unheated-cylinder wake. (c) Time-averaged temperature T_{ave}/T_0 and (d) rms temperature fluctuation T_{rms}/T_0 of the heated-cylinder wake. See Table I for symbols.

IV. RESULTS AND DISCUSSIONS

A. Characteristics of the cylinder wakes

Prior to the experiments of the interaction between the shock wave and the cylinder wake, the velocity characteristics of the unheated-cylinder wakes and the temperature characteristics of the heated-cylinder wakes are examined without the shock wave ejections. In the unheated-cylinder wake, the streamwise velocity is measured with the hot-wire probe in the vertical direction at 561 mm ($\approx 47D$) downstream from the cylinder. Here, the vertical coordinate is denoted with y ($y = 0$ is the cylinder center location). Note that the measurements are conducted at the same streamwise location of the intersection of the wake centerline and the shock ray [see the red cross in Fig. 1(b)]. At each point, instantaneous velocity U or temperature T is measured over 26 s, and the statistics are calculated with the time average, denoted by the subscript "ave."

Figures 3(a) and 3(b) show mean velocity U_{ave} and root-mean-squared (rms) velocity fluctuation $u_{rms} = \sqrt{(U^2)_{ave} - U_{ave}^2}$ in the unheated-cylinder wake, respectively. The velocity defect $\Delta U = U_0 - U_{ave}$ is the largest near the wake center ($y/D = 0$) and becomes smaller as $|y/D|$ becomes larger, as expected. The half-width of the wake based on ΔU, b_U is about 30 mm, which corresponds to $|y/D| \approx 2.5$. u_{rms} has a small peak at the half-width location and decreases with y/D. Qualitatively similar profiles were confirmed for the streamwise velocity defect and rms velocity fluctuation in a previous study on a heated-cylinder wake [42].

Figures 3(c) and 3(d) show mean temperature T_{ave} and rms temperature fluctuation $T_{rms} = \sqrt{(T^2)_{ave} - T_{ave}^2}$ of the heated-cylinder wake. In addition to ΔU, the temperature deviation from room temperature T_0, $\Delta T = T_{ave} - T_0$, also has a peak at the wake center. Apparently, the half-width based on ΔT, b_T is larger than that on ΔU, in agreement with previous studies [34,42]. The peak of

TABLE II. Skewness and flatness of u for the unheated cases (cases 1-OFF, 2-OFF, and 3-OFF) and those of T' for the heated cases (cases 1-ON, 2-ON, and 3-ON).

Case	1-OFF 1-ON	2-OFF 2-ON	3-OFF 3-ON
Skewness	−0.142	0.150	0.0373
	1.05	0.783	0.327
Flatness	2.96	2.95	2.75
	4.95	4.14	3.17

$T_{\rm rms}$ is also obtained at larger y/D than that of $u_{\rm rms}$, which is also the same tendency as that of the previous studies on heated-cylinder wakes [42,43].

These measurement results are summarized in Table I, which shows the velocity and temperature statistics measured at the intersection of the cylinder wake centerline and the shock ray. This intersection point is shown in Fig. 1 as a red cross. Here, as the Richardson number is small enough for the temperature to be passive to the velocity field, the velocity statistics in the heated-cylinder experiments can be assumed to be the same as in the unheated-cylinder experiments with the same U_0. The Taylor microscale is defined as

$$\lambda^2 = \frac{u_{\rm rms}^2}{U_{\rm ave}^2 (\partial u/\partial t)_{\rm ave}^2}, \tag{17}$$

where Taylor's hypothesis is used to replace the spatial derivative $\partial/\partial x$ in the denominator in the original definition of λ with time derivative. Taylor's hypothesis is also applied to the calculation of the longitudinal velocity integral length scale L_u as

$$L_u = \int_0^\infty \frac{[u(t)u(t+\tau)]_{\rm ave}}{u_{\rm rms}^2} U_{\rm ave} d\tau. \tag{18}$$

The longitudinal temperature integral length scale L_T is calculated by integrating the autocorrelation function of the temperature fluctuation $T' = T - T_{\rm ave}$. Hereafter, the cylinder wake characteristics of each case are represented as the values shown in Table I.

Table II summarizes the skewness and flatness of u for the unheated cases and those of T' for the heated cases. The skewness and flatness of u are close to the Gaussian values (0 and 3, respectively) from a previous study on cylinder wakes for the streamwise distance from the cylinder center $x \geqslant 10D$ (at the wake centerline) [44]. The skewness and flatness of T', on the other hand, show larger values than 0 and 3, respectively. It is known that the skewness and flatness of the temperature fluctuations of a wake are larger than the Gaussian values in the near wake region, which are associated with the von Karman vortices, where the cool fluid outside the wake is entrained in the warm fluid inside the wake [45–48]. Our experimental results are consistent with the previous experimental study of a heated-cylinder wake, where the skewness and flatness of temperature fluctuations were larger than 0 and 3, respectively, for $x \leqslant 75D$ [46].

B. Average of peak overpressure

Time histories of the overpressure in cases 1-OFF, 1-ON, 3-OFF, and 3-ON are shown in Fig. 4 as examples. In all cases, the overpressure reaches a peak with a short rise time upon arrival of the shock wave. Subsequently, the overpressure gradually decreases because of the expansion wave that follows the spherical shock wave. While the overpressure decreases, another peak appears again in all cases. The second peak is due to the shock wave reflected by the hot-wire probe (or cold-wire probe) as reported in our previous study [33]. By comparing Figs. 4(a) and 4(b) [or Figs. 4(c) and 4(d)], we can find that the instantaneous pressure waveforms are qualitatively the same in the unheated/heated cases. From the comparison of Figs. 4(a) and 4(c) [or Figs. 4(b) and 4(d)], the first

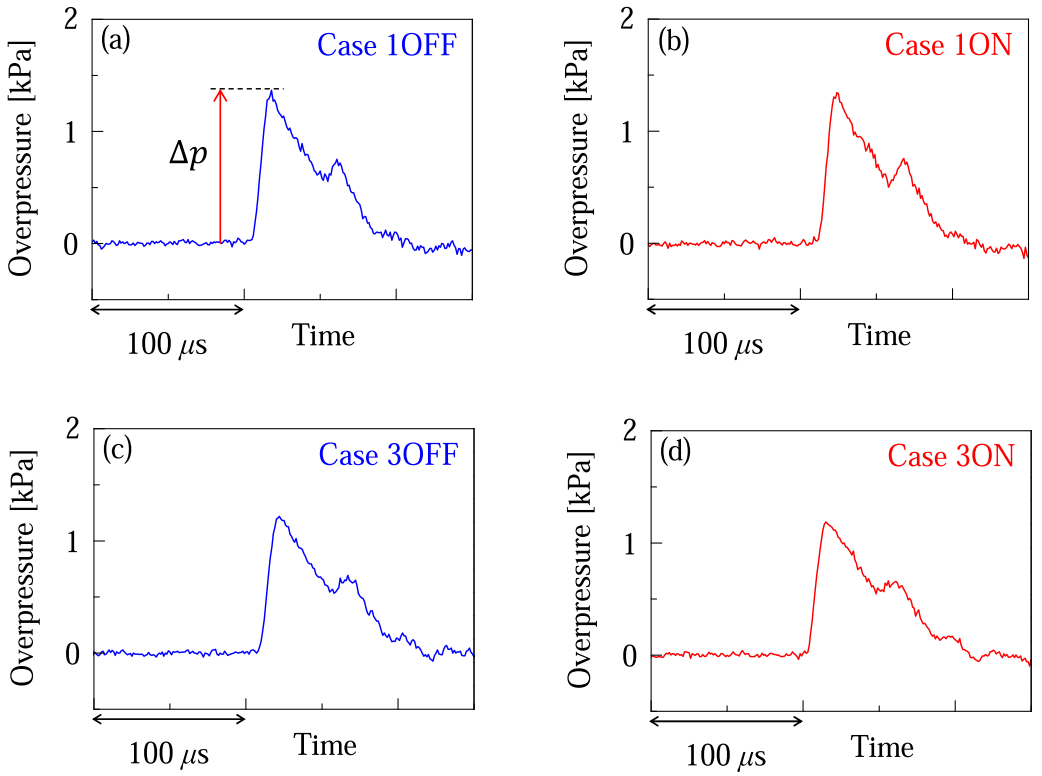

FIG. 4. Examples of pressure waveforms in cases (a) 1-OFF, (b) 1-ON, (c) 3-OFF, and (d) 3-ON.

peak seems to become slightly rounder and smaller in the cylinder wake with larger U_0. Here, we define the peak overpressure Δp with the first peak in overpressure signals as shown in Fig. 4(a). The characteristics of Δp are investigated in this paper.

In Fig. 5(a), the ensemble averages of peak overpressure $\langle \Delta p \rangle$ are plotted against the velocity defect ΔU, where $\langle \Delta p \rangle$ decreases with ΔU. Here, the ensemble average is taken with 400 ejections

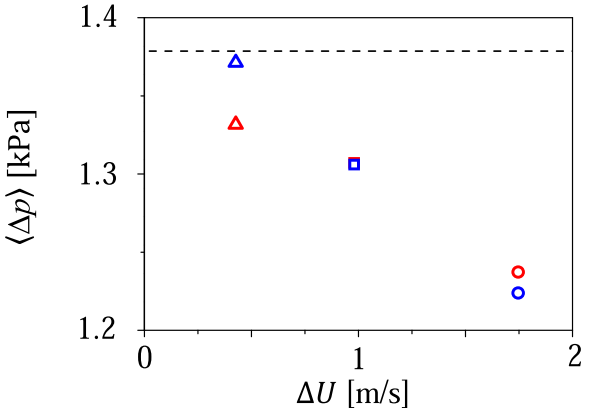

FIG. 5. $\langle \Delta p \rangle$ plotted against ΔU. The broken line shows $\langle \Delta p \rangle$ obtained in the flow at $U_0 = 10$ m/s without the cylinder. See Table I for symbols.

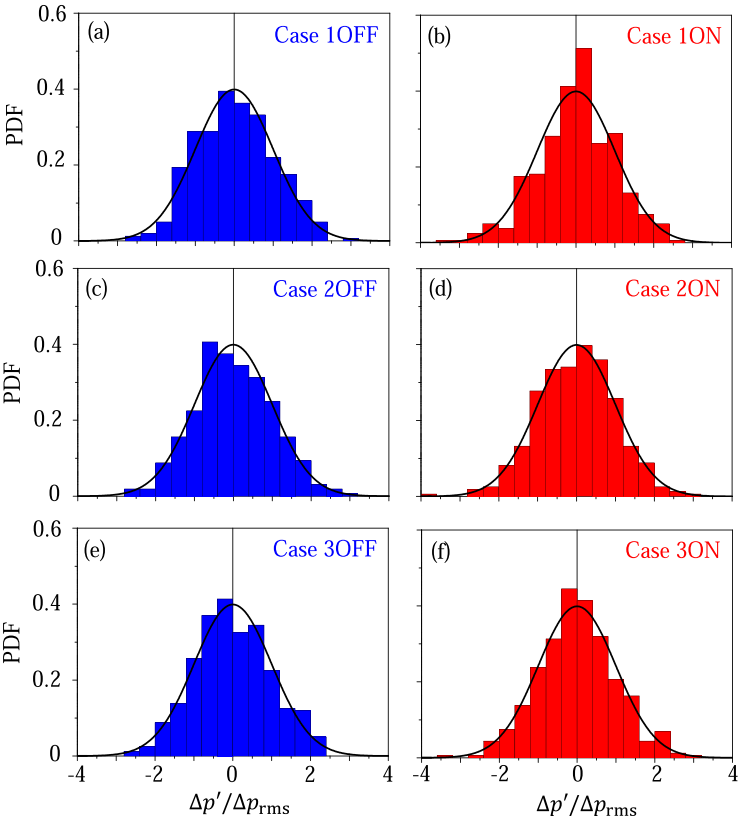

FIG. 6. PDFs of cases (a) 1-OFF, (b) 1-ON, (c) 2-OFF, (d) 2-ON, (d) 3-OFF, and (f) 3-ON. Solid lines show the Gaussian profile. See Table I for symbols.

of the shock wave. The broken line represents $\langle \Delta p \rangle$ obtained in a laminar flow at $U_0 = 10$ m/s without the cylinder ($\Delta U \approx 0$ m/s). $\langle \Delta p \rangle$ is decreased by the cylinder wake. $\langle \Delta p \rangle$ in case 3-OFF is decreased by 11% from the broken line, which is the largest of all cases. This has been explained in previous experiments on shock waves propagating in a turbulent wake [33]. Because of the velocity defect in the wake, the shock wave in the wake tends to move faster than outside the wake in the present experimental setup, resulting in a convex shape of the shock wave surface in the shock propagation direction. The convex shape causes a defocusing effect that weakens the shock wave, namely a decrease in the peak overpressure [49]. A significant drop in $\langle \Delta p \rangle$ appears in case 1-ON, whose ΔT is the largest among all the heated cases, where $\langle \Delta p \rangle$ of case 1-ON is 3% smaller than that of case 1-OFF. The drop in $\langle \Delta p \rangle$ can be caused by the shock wave propagation in the wake region where the averaged temperature is increased by ΔT; positive ΔT induces the increase in sound speed a in front of the shock wave and the convex shape of the shock wave surface in the shock propagation direction, resulting in a decrease in $\langle \Delta p \rangle$ (shock wave deformation similar to that shown in Fig. 2 occurs, but a temperature increase ΔT is considered in front of the shock wave instead of T'). It can be considered that ΔT for cases 2-ON and 3-ON is not large compared to that for case 1-ON so that the effects of ΔT do not significantly change in $\langle \Delta p \rangle$.

C. Statistics of peak-overpressure fluctuations

Figure 6 shows probability density functions (PDFs) of $\Delta p' = \Delta p - \langle \Delta p \rangle$, which follow well the Gaussian profile. The skewness ($\langle \Delta p'^3 \rangle / \Delta p'^3_{\rm rms}$) and flatness ($\langle \Delta p'^4 \rangle / \Delta p'^4_{\rm rms}$) obtained in all

TABLE III. Skewness and flatness of $\Delta p'$.

Case 1-ON	1-OFF 2-ON	2-OFF 3-ON	3-OFF
Skewness	0.0642	0.138	0.198
	−0.235	−0.0984	0.0422
Flatness	2.70	2.87	3.05
	3.18	3.13	3.07

cases are compared in Table III. Both in the heated and unheated cases, the skewness and flatness are close to the Gaussian values (0 and 3, respectively). It is remarkable that the skewness and flatness become smaller and larger, respectively, in the heated-cylinder cases compared to the unheated-cylinder cases. As described in the shock deformation model, positive/negative $\Delta p'$ can be caused by the concave/convex shock deformation in the propagation direction, which is induced by negative/positive a' (or T') in front of the shock wave. Therefore, it can be assumed that the probability distribution of $\Delta p'$ is closely related to that of T'. Namely, when the probability distribution of T' is positively skewed, the skewness of $\Delta p'$ becomes smaller since $\Delta p'$ is a decreasing function of T' according to Eq. (9). In addition, the larger flatness of T' than the Gaussian value makes the flatness of $\Delta p'$ larger. As shown in Table II, the skewness and flatness of T' for the heated-cylinder wakes are larger than the Gaussian values. Indeed, in the present experiments, the skewness and flatness of $\Delta p'$ for the heated cases are smaller and larger, respectively, than those for the unheated cases, consistent with the above assumption.

The rms value of the peak-overpressure fluctuations is defined by $\Delta p_{\mathrm{rms}} = \langle \Delta p'^2 \rangle^{1/2}$. The peak-overpressure fluctuations induced by the cylinder wake are of interest in this study, although Δp_{rms} contains contributions from fluctuations caused by noise in pressure transducer signals and variations of the shock wave characteristics due to imperfect repeatability of the shock wave generator. These effects are also discussed in detail in Ref. [11]. The contribution of the fluctuations inherently caused in the experimental facility is evaluated by an experiment without cylinders, i.e., a shock wave propagating in a laminar flow. Δp_{rms} obtained in this experiment is denoted by $(\Delta p_{\mathrm{rms}})_{\mathrm{w/o}}$. The peak-overpressure fluctuations induced by the cylinder wake are evaluated as $\sigma_{\Delta p} = [\Delta p_{\mathrm{rms}}^2 - (\Delta p_{\mathrm{rms}})_{\mathrm{w/o}}^2]^{1/2}$ following the previous study [11,12].

Figures 7(a)–7(d) plot $\sigma_{\Delta p}/\langle \Delta p \rangle$ against $f/\sqrt{M_{\mathrm{S0}}^2 - 1}$, where $f = f(u_{\mathrm{rms}}/a_0, 0, 0)$, $f = f(u_{\mathrm{rms}}/a_0, T_{\mathrm{rms}}/2T_0, 0)$, $f = f(u_{\mathrm{rms}}/a_0, T_{\mathrm{rms}}/2T_0, 0.5)$, and $f = f(u_{\mathrm{rms}}/a_0, T_{\mathrm{rms}}/2T_0, 1)$ of Eq. (12), respectively. R^2 in each figure shows the coefficient of determination calculated between Eq. (13), drawn with the solid line, and the experimental data. f is a function of u_{rms}/a_0, $T_{\mathrm{rms}}/2T_0$, and C_{uT}. Note that u_{rms}/a_0 and $T_{\mathrm{rms}}/2T_0$ are the values measured in our experiments, while C_{uT} is not measured and is unknown in the present experiments. Since in a heated-cylinder wake u and T' are positively correlated (the positive u direction is the opposite of the wake streamwise direction here) [42], we can say that $0 \leqslant C_{uT} \leqslant 1$. In Fig. 7, $C_{uT} = 0$, 0.5, and 1 are assumed as explained below. The temperature fluctuation T' is not taken into account in Fig. 7(a), which was also derived in Ref. [12]. Figure 7(b) includes the effect of temperature fluctuations as T_{rms} but ignores the correlation between u and T' ($C_{uT} = 0$). Figures 7(c) and 7(d) consider the correlation as $C_{uT} = 0.5$ and 1, respectively. We can find that in Fig. 7(a), $\sigma_{\Delta p}/\langle \Delta p \rangle$ of cases 1-OFF through 3-OFF increases with u_{rms}, consistent with our previous studies [11,12]. It is also found that $\sigma_{\Delta p}/\langle \Delta p \rangle$ in cases 1-ON through 3-ON are larger than those in cases 1-OFF through 3-OFF, respectively, which confirms that the temperature fluctuations result in an increase in the overpressure fluctuations as seen in Ref. [30]. Comparing Figs. 7(b), 7(c) and 7(d) with Fig. 7(a), it is obvious that by considering the contribution of T' on $\Delta p'$, $\sigma_{\Delta p}/\langle \Delta p \rangle$ correlates stronger with the model prediction by Eq. (13). The largest R^2 is found between $\sigma_{\Delta p}/\langle \Delta p \rangle$ and $(u_{\mathrm{rms}}/a_0 + T_{\mathrm{rms}}/2T_0)/\sqrt{M_{\mathrm{S0}}^2 - 1}$ with $C_{uT} = 1$. It should

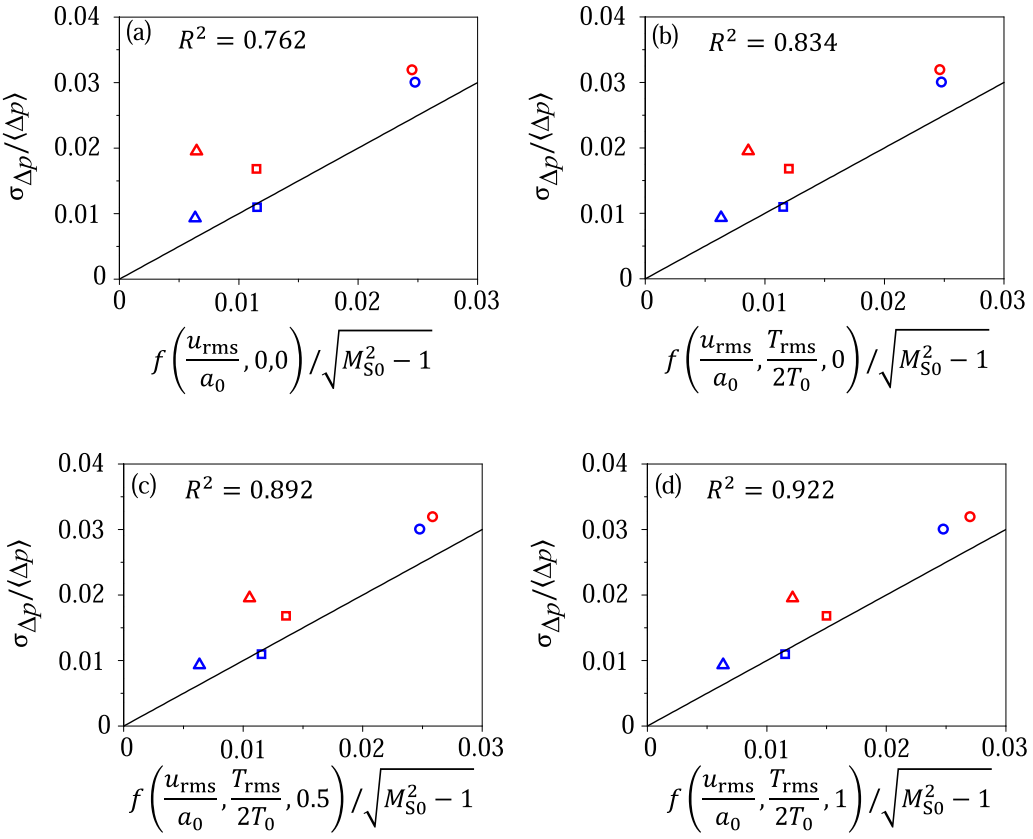

FIG. 7. $\sigma_{\Delta p}/\langle\Delta p\rangle$ plotted against (a) $f(u_{\rm rms}/a_0, 0, 0)/\sqrt{M_{S0}^2 - 1}$, (b) $f(u_{\rm rms}/a_0, T_{\rm rms}/2T_0, 0)/\sqrt{M_{S0}^2 - 1}$, (c) $f(u_{\rm rms}/a_0, T_{\rm rms}/2T_0, 0.5)/\sqrt{M_{S0}^2 - 1}$, and (d) $f(u_{\rm rms}/a_0, T_{\rm rms}/2T_0, 1)/\sqrt{M_{S0}^2 - 1}$. Solid lines in each figure are calculated with Eq. (11). The coefficients of determination R^2 calculated between $\sigma_{\Delta p}/\langle\Delta p\rangle$ and $f/\sqrt{M_{S0}^2 - 1}$ of each figure are also shown. See Table I for symbols.

be noted that $\langle\Delta p\rangle$ is decreased past the cylinder wake in our experiments as mentioned above, while the reduction of $\langle\Delta p\rangle$ is ignored in Eq. (16). This can be the reason why $\sigma_{\Delta p}/\langle\Delta p\rangle$ is slightly larger than Eq. (16) in Fig. 7(c). Since Eq. (16) is derived by the shock deformation model, we can say that the deformation of the shock wave surface caused by the interaction with the temperature fluctuation plays an important role for the overpressure fluctuation behind the shock wave.

Here, we should note that spherical shock waves are used in the present study, while most previous studies considered planar shock waves for shock-turbulence interactions [8,9,15,20]. Since a spherical shock wave has a finite curvature radius, the effects of the spherical shape on the shock-turbulence interaction become large when the ratio of the curvature radius and characteristic length scales of turbulence is small. Conversely, when the curvature radius is large enough compared to the turbulence length scales, the spherical shock wave–turbulence interaction is geometrically equivalent to a planar shock wave–turbulence interaction. The curvature radius of the present spherical shock wave is 276 mm at the intersection of the wake centerline and the shock ray [see the red cross in Fig. 1(b)], which is much larger than the characteristic turbulence length scales of the cylinder wakes such as λ and L_u (4.45 and 59.4 mm, respectively, at the largest in the six cases). Indeed, in our previous studies on interactions between the spherical shock wave and grid turbulence [11,12], where the ratio of the curvature radius and λ (or L_u) was similar to that of the present study, the dependence of Δp fluctuations on shock Mach number M_{S0} and turbulent Mach

number M_T was consistent with that in planar shock wave-turbulence interactions investigated by direct numerical simulations [50]. Thus, the effects of the spherical shape on the interaction can be assumed to be small enough in the present experiments.

D. Correlation between the velocity/temperature and overpressure fluctuations

Correlation coefficients between velocity and peak-overpressure fluctuations are calculated for experiments with the unheated-cylinder wake following our previous study [31,33]. The Taylor's hypothesis is used for estimating the spatial distribution of velocity $U(d)$ along the wake centerline from the time history of velocity $U(t)$. Here, the direction of positive U is the same as the wake streamwise direction. The streamwise distance between the pressure transducer location d is given by $d = -U_0 t - \Delta_{\mathrm{HP}}$, where $\Delta_{\mathrm{HP}} = 10$ mm is the streamwise distance between the hot-wire probe and the pressure transducer, and in each time series data of $U(t)$, $t = 0$ is defined such that $U(d)$ represents the velocity distribution at the moment of the shock wave ejection [33]. As the shock wave propagation is much faster than advection of the wake, the shock wave is assumed to propagate in a flow whose velocity on the wake centerline is given by $U(d)$. Furthermore, the low-pass filter is applied to $U(d)$ with a cutoff length of Δd as

$$\overline{U}(d, \Delta d) = \frac{1}{\Delta d} \int_{-\Delta d/2}^{\Delta d/2} U(d + \delta) d\delta, \tag{19}$$

which represents velocity at scales larger than Δd at the location d. The velocity fluctuation above the scale Δd is $\hat{u}(d, \Delta d) = U_{\mathrm{ave}} - \overline{U}(d, \Delta d)$. The correlation coefficient R_u is calculated between $\hat{u}$ and $\Delta p'$ as

$$R_u(d, \Delta d) = \frac{\langle \hat{u} \Delta p' \rangle}{\sqrt{\langle \hat{u}^2 \rangle \langle \Delta p'^2 \rangle}}. \tag{20}$$

In the same way, the correlation coefficient is calculated between large-scale temperature fluctuation and peak-overpressure fluctuation from the heated-cylinder experiments. The temperature profile along the wake centerline, $T(d)$, is estimated from the time history of temperature $T(t)$ measured with a cold-wire probe. The low pass-filtered temperature is obtained as follows:

$$\overline{T}(d, \Delta d) = \frac{1}{\Delta d} \int_{-\Delta d/2}^{\Delta d/2} T(d + \delta) d\delta. \tag{21}$$

The temperature fluctuation above the scale Δd is $\hat{T}'(d, \Delta d) = \overline{T}(d, \Delta d) - T_{\mathrm{ave}}$. The correlation coefficient between $\hat{T}'$ and $\Delta p'$, R_T is calculated as

$$R_T(d, \Delta d) = \frac{\langle \hat{T}' \Delta p' \rangle}{\sqrt{\langle \hat{T}'^2 \rangle \langle \Delta p'^2 \rangle}}. \tag{22}$$

R_u and R_T in all cases are shown as functions of d and Δd in Fig. 8. As in Figs. 8(a), 8(c) and 8(e), the velocity fluctuations and peak-overpressure fluctuations are negatively correlated. Note that the direction of positive $\hat{u}$ is opposite to the wake streamwise direction. This indicates that velocity fluctuations opposing the shock propagation increase the peak-overpressure, and vice versa. The same tendency was found in previous studies, where planar or spherical shock waves propagate in grid turbulence or isotropic turbulence [21,31]. As seen in Figs. 8(b), 8(d) and 8(f), negative correlation can also be found between the temperature and peak-overpressure fluctuations, suggesting that an increase in temperature in front of the shock wave causes a decrease in the peak overpressure, and vice versa. A qualitatively similar effect was reported for a laser-induced hot fluid generated in front of a shock wave, where the fluid with high temperature attenuates pressure behind the shock wave [51].

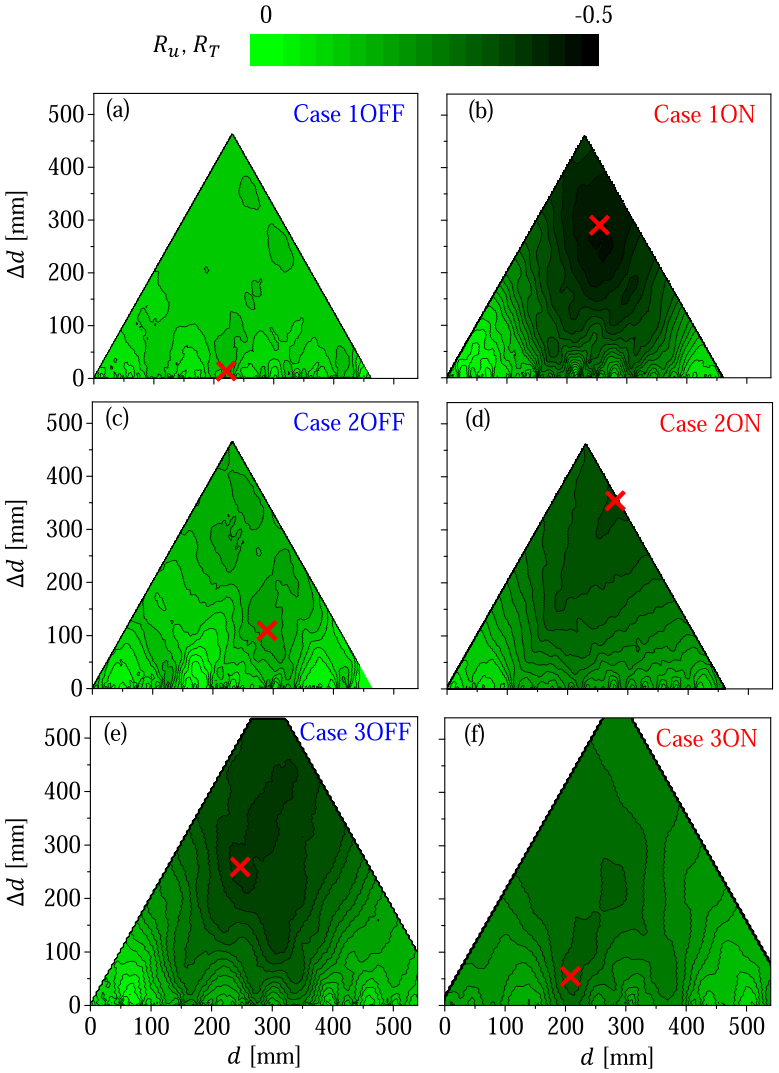

FIG. 8. Correlation coefficients $R_u(d, \Delta d)$ and $R_T(d, \Delta d)$ of cases (a) 1-OFF, (b) 1-ON, (c) 2-OFF, (d) 2-ON, (d) 3-OFF, and (e) 3-ON. Note that R_u is shown in (a), (c), and (e) while R_T is shown in (b), (d), and (f). The crosses show $(d_{\max}, \Delta d_{\max})$.

The negative correlation between velocity and peak overpressure is explained well by the shock deformation model [31,33], which is now used to assess the effects of temperature fluctuations on $\Delta p'$. Figures 9(a) and 9(b) show the schematic of the shock deformation caused by the interaction with the positive and negative temperature fluctuations, respectively. As in Eq. (5), negative/positive temperature fluctuation T' (negative/positive sound speed fluctuation a') results in the local decrease/increase of the shock movement velocity, which makes the shock wave surface concave/convex in the propagation direction, respectively. And as in Eq. (9), negative/positive T' yields positive/negative $\Delta p'$. Thus, T' and $\Delta p'$ are negatively correlated.

We define the maximum absolute values of R_u and R_T in each case as $(R_u)_{\max}$ and $(R_T)_{\max}$, respectively. Red crosses in Fig. 8 mark $(d, \Delta d) = (d_{\max}, \Delta d_{\max})$, where $(R_u)_{\max}$ or $(R_T)_{\max}$ is obtained. $\Delta d_{\max}$ was found to be of the same order of L_u in previous studies on a shock wave interacting

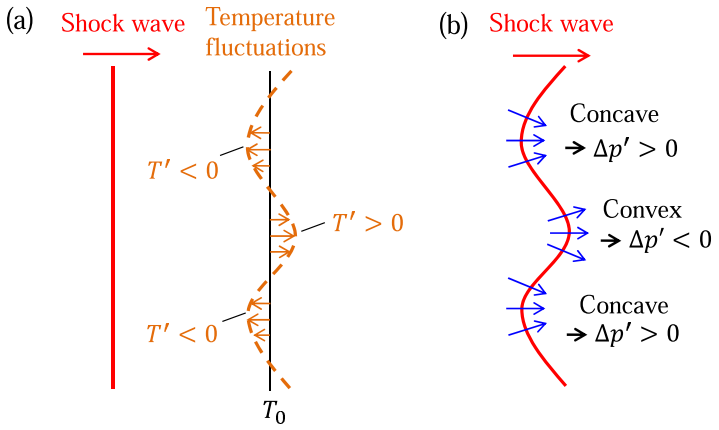

FIG. 9. (a) Schematic of the shock wave surface and the temperature fluctuating field in front of the shock wave before the interaction. (b) Shock wave deformation caused by the interaction.

with grid turbulence [31], cylinder wake(s) [32,33], and homogeneous isotropic turbulence [21,50]. The result that $\Delta d_{\max}$ is of the order of L_u is also obtained in the unheated-cylinder wake cases in the present study, which shows that large-scale turbulent eddies are important in the modulation of the shock wave. We also find that it is mostly of the same order of L_T in the heated-cylinder wake cases, suggesting that large-scale temperature fluctuations are important in the shock wave modulation.

In Fig. 10, $d_{\max}$ of all the cases are compared with the shock ray. Note that h is the vertical distance from the pressure transducer, and the velocity/temperature measurement point is at $h = 75$ mm in all the cases. $d_{\max}$ is located near the ray, and temperature and velocity fluctuations on the shock ray have a strong influence on the shock wave. Figure 11 shows the relation between $(R_u)_{\max}$ and $u_{\rm rms}/a_0$ and the relation between $(R_T)_{\max}$ and $T_{\rm rms}/2T_0$. The lateral axis represents both $u_{\rm rms}/a_0$ and $T_{\rm rms}/2T_0$ since they are comparable with respect to the contribution to $\Delta p'$ as in Eq. (9). It is discovered that $|(R_u)_{\max}|$ and $|(R_T)_{\max}|$ increase with $u_{\rm rms}/a_0$ and $T_{\rm rms}/2T_0$, respectively, indicating that the larger the velocity or temperature fluctuations at a specific point on the ray, the more significant their influence on $\Delta p'$ becomes compared with the influence of fluctuations at other points on the ray. It is interesting that when $u_{\rm rms}/a_0$ and $T_{\rm rms}/2T_0$ are in the same order, $|(R_T)_{\max}|$ is larger than $|(R_u)_{\max}|$. This can be explained with the correlation of u and T' in the heated-cylinder wake. Both $T' < 0$ and $u < 0$ tend to amplify $\Delta p'$ as confirmed by the correlations in Fig. 8 while their positive fluctuations attenuate $\Delta p'$. Since u and T' are positively correlated

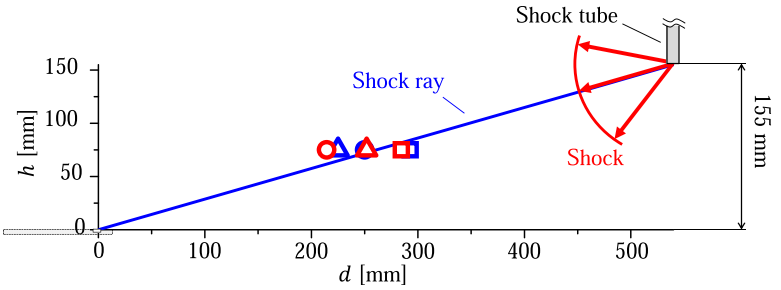

FIG. 10. Relation between $d_{\max}$ and the shock ray from the open end of the shock tube to the pressure transducer location. See Table I for symbols.

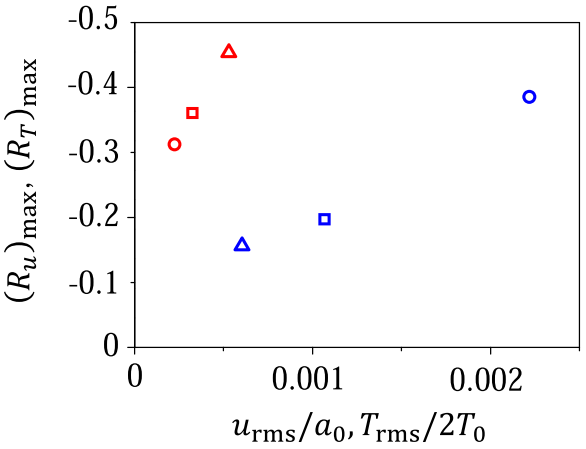

FIG. 11. Relation between $(R_u)_{\max}$ and $u_{\rm rms}/a_0$ (blue) and relation between $(R_T)_{\max}$ and $T_{\rm rms}/2T_0$ (red) in each case. See Table I for symbols.

in the heated-cylinder wake [42], the temperature effect on $\Delta p'$ is piled on the velocity effect according to Eq. (9). Thus, instantaneous $\Delta p'$ is amplified both by u and T' in the heated-cylinder wake cases, while $\Delta p'$ is caused only by u in the unheated-cylinder wake cases, resulting in $|(R_T)_{\max}| > |(R_u)_{\max}|$.

V. CONCLUDING REMARKS

In this study, we have investigated the effects of velocity and temperature fluctuations on the shock wave modulation in wind tunnel experiments on a spherical shock wave propagating in unheated/heated-cylinder wakes. We have conducted the overpressure measurements behind the shock wave, where the instantaneous velocity or temperature of the wake that interacts with the shock wave has also been measured. In both the unheated- and heated-cylinder wake cases, the ensemble average of peak overpressure decreases with the velocity defect of the cylinder wakes. The averaged peak overpressure for case 1-ON is 3% smaller than that for case 1-OFF, while a significant change in the averaged peak overpressure has not been found for cases 2-ON and 3-ON. Smaller skewness and larger flatness have been obtained in the PDFs of overpressure fluctuations in the heated-cylinder wakes than those in the unheated-cylinder wake cases. In the heated-cylinder wake cases, the rms peak-overpressure fluctuation has been increased from that of the unheated-cylinder wake cases, and the coefficient of variation of the peak overpressure has been represented as a function of the rms velocity fluctuations, rms temperature fluctuations, and the correlation coefficient of the velocity and temperature fluctuations, which has been derived with the shock deformation model, where the velocity and temperature fluctuations are normalized to be compared with each other. From the calculation of the correlation coefficients between the temperature and overpressure fluctuations, it has been found that the temperature and peak-overpressure fluctuations are negatively correlated, meaning that peak overpressure is increased/decreased after interacting with the negative/positive temperature fluctuation. The absolute value of the correlation coefficients has been found to become larger as $T_{\rm rms}$ increases. It has also been uncovered that when the normalized temperature fluctuations in the heated cylinder cases are the same order with the normalized velocity fluctuations in the unheated cylinder cases, the correlation coefficients between the temperature and ovepressure fluctuations in the heated-cylinder cases are larger than the correlation coefficients between the velocity and overpressure fluctuations in the unheated-cylinder cases. This is because in the heated-cylinder cases, the overpressure fluctuations are modulated both by the velocity and the temperature fluctuations due to the correlation between the velocity and

temperature in the heated-cylinder wake, while in the unheated-cylinder wake they are modulated only by the velocity fluctuations.

ACKNOWLEDGMENTS

We thank A. Sasoh, A. Murata, and K. Mori for their help and valuable comments on this work. Part of this work was supported by JSPS KAKENHI Grants No. 18J21758, No. 18H01367, No. 18H01369, and No. 18K13682.

[1] M.-M. Mac Low and R. S. Klessen, Control of star formation by supersonic turbulence, Rev. Mod. Phys. **76**, 125 (2004).
[2] V. A. Thomas and R. J. Kares, Drive Asymmetry and the Origin of Turbulence in an ICF Implosion, Phys. Rev. Lett. **109**, 075004 (2012).
[3] D. J. Maglieri, Some effects of airplane operations and the atmosphere on sonic-boom signatures, J. Acoust. Soc. Am. **39**, S36 (1966).
[4] H. L. Seegmiller, J. G. Marvin, and L. L. Levy, Jr., Steady and unsteady transonic flow, AIAA J. **16**, 1262 (1978).
[5] J. M. Delery, Shock wave/turbulent boundary layer interaction and its control, Prog. Aerosp. Sci. **22**, 209 (1985).
[6] D. S. Dolling, Fifty years of shock-wave/boundary-layer interaction research: What next? AIAA J. **39**, 1517 (2001).
[7] L. Agostini, L. Larchevêque, and P. Dupont, Mechanism of shock unsteadiness in separated shock/boundary-layer interactions, Phys. Fluids **27**, 126103 (2015).
[8] J. Keller and W. Merzkirch, Interaction of a normal shock wave with a compressible turbulent flow, Exp. Fluids **8**, 241 (1990).
[9] J. H Agui, G. Briassulis, and Y. Andreopoulos, Studies of interactions of a propagating shock wave with decaying grid turbulence: Velocity and vorticity fields, J. Fluid Mech. **524**, 143 (2005).
[10] T. Kitamura, K. Nagata, Y. Sakai, A. Sasoh, and Y. Ito, Changes in divergence-free grid turbulence interacting with a weak spherical shock wave, Phys. Fluids **29**, 065114 (2017).
[11] A. Sasoh, T. Harasaki, T. Kitamura, D. Takagi, S. Ito, A. Matsuda, K. Nagata, and Y. Sakai, Statistical behavior of post-shock overpressure past grid turbulence, Shock Waves **24**, 489 (2014).
[12] K. Inokuma, T. Watanabe, K. Nagata, and Y. Sakai, Statistics of overpressure fluctuations behind a weak shock wave interacting with turbulence, Phys. Fluids **31**, 085119 (2019).
[13] B. Lipkens and D. T. Blackstock, Model experiment to study sonic boom propagation through turbulence. Part I. general results, J. Acoust. Soc. Am. **103**, 148 (1998).
[14] J.-H. Kim, A. Sasoh, and A. Matsuda, Modulations of a weak shock wave through a turbulent slit jet, Shock Waves **20**, 339 (2010).
[15] T. Tamba, G. Fukushima, M. Kayumi, A. Iwakawa, and A. Sasoh, Experimental investigation of the interaction of a weak planar shock with grid turbulence in a counter-driver shock tube, Phys. Rev. Fluids **4**, 073401 (2019).
[16] S. Lee, S. K. Lele, and P. Moin, Direct numerical simulation of isotropic turbulence interacting with a weak shock wave, J. Fluid Mech. **251**, 533 (1993).
[17] J. Larsson and S. K. Lele, Direct numerical simulation of canonical shock/turbulence interaction, Phys. Fluids **21**, 126101 (2009).
[18] D. A. Donzis, Amplification factors in shock-turbulence interactions: Effect of shock thickness, Phys. Fluids **24**, 011705 (2012).
[19] D. A. Donzis, Shock structure in shock-turbulence interactions, Phys. Fluids **24**, 126101 (2012).
[20] J. Larsson, I. Bermejo-Moreno, and S. K. Lele, Reynolds- and mach-number effects in canonical shock-turbulence interaction, J. Fluid Mech. **717**, 293 (2013).

[21] K. Tanaka, T. Watanabe, K. Nagata, A. Sasoh, Y. Sakai, and T. Hayase, Amplification and attenuation of shock wave strength caused by homogeneous isotropic turbulence, Phys. Fluids **30**, 035105 (2018).
[22] C. H. Chen and D. A. Donzis, Shock–turbulence interactions at high turbulence intensities, J. Fluid Mech. **870**, 813 (2019).
[23] Y. P. M. Sethuraman and K. Sinha, Effect of turbulent mach number on the thermodynamic fluctuations in canonical shock-turbulence interaction, Comput. Fluids **197**, 104354 (2020).
[24] K. Mahesh, S. K. Lele, and P. Moin, The influence of entropy fluctuations on the interaction of turbulence with a shock wave, J. Fluid Mech. **334**, 353 (1997).
[25] P. Moin and K. Mahesh, Direct numerical simulation: A tool in turbulence research, Annu. Rev. Fluid Mech. **30**, 539 (1998).
[26] S. Jamme, J.-B. Cazalbou, F. Torres, and P. Chassaing, Direct numerical simulation of the interaction between a shock wave and various types of isotropic turbulence, Flow, Turbul. Combust. **68**, 227 (2002).
[27] J. Ryu and D. Livescu, Turbulence structure behind the shock in canonical shock–vortical turbulence interaction, J. Fluid Mech. **756** (2014).
[28] B. McManamen, D. A. Donzis, S. W. North, and R. D. W. Bowersox, Velocity and temperature fluctuations in a high-speed shock–turbulence interaction, J. Fluid Mech. **913** A10 (2021).
[29] L. S. G. Kovasznay, Turbulence in supersonic flow, J. Aeronaut. Sci. **20**, 657 (1953).
[30] E. Salze, P. Yuldashev, S. Ollivier, V. Khokhlova, and P. Blanc-Benon, Laboratory-scale experiment to study nonlinear N-wave distortion by thermal turbulence, J. Acoust. Soc. Am. **136**, 556 (2014).
[31] K. Inokuma, T. Watanabe, K. Nagata, A. Sasoh, and Y. Sakai, Finite response time of shock wave modulation by turbulence, Phys. Fluids **29**, 051701 (2017).
[32] K. Inokuma, T. Watanabe, K. Nagata, and Y. Sakai, Statistical properties of spherical shock waves propagating through grid turbulence, turbulent cylinder wake, and laminar flow, Phys. Scr. **94**, 044004 (2019).
[33] K. Aruga, K. Inokuma, T. Watanabe, K. Nagata, and Y. Sakai, Experimental investigation of interactions between turbulent cylinder wake and spherical shock wave, Phys. Fluids **32**, 016101 (2020).
[34] P. Freymuth and M. S. Uberoi, Structure of temperature fluctuations in the turbulent wake behind a heated cylinder, Phys. Fluids **14**, 2574 (1971).
[35] Y. Zhou and R. A. Antonia, Convection velocity measurements in a cylinder wake, Exp. Fluids **13**, 63 (1992).
[36] H. Hu and M. M. Koochesfahani, Thermal effects on the wake of a heated circular cylinder operating in mixed convection regime, J. Fluid Mech. **685**, 235 (2011).
[37] R. M. Fand and K. K. Keswani, Combined natural and forced convection heat transfer from horizontal cylinders to water, Int. J. Heat Mass Transf. **16**, 1175 (1973).
[38] V. T. Morgan, The overall convective heat transfer from smooth circular cylinders, Adv. Heat Transf. **11**, 199 (1975).
[39] F. Dumouchel, J. C. Lecordier, and P. Paranthoën, The effective reynolds number of a heated cylinder, Int. J. Heat Mass Transf. **41**, 1787 (1998).
[40] A.-B. Wang, Z. Trávníček, and K.-C. Chia, On the relationship of effective reynolds number and strouhal number for the laminar vortex shedding of a heated circular cylinder, Phys. Fluids **12**, 1401 (2000).
[41] G. B. Whitham, A new approach to problems of shock dynamics part i two-dimensional problems, J. Fluid Mech. **2**, 145 (1957).
[42] H. S. Kang and C. Meneveau, Universality of large eddy simulation model parameters across a turbulent wake behind a heated cylinder, J. Turbul. **3**, N32 (2002).
[43] G. Fabris, Conditional sampling study of the turbulent wake of a cylinder. part 1, J. Fluid Mech. **94**, 673 (1979).
[44] M. J. E. Yazdi and A. B. Khoshnevis, Comparing the wake behind circular and elliptical cylinders in a uniform current, SN Appl. Sci. **2**, 994 (2020).
[45] K. R. Sreenivasan, Evolution of the centerline probability density function of temperature in a plane turbulent wake, Phys. Fluids **24**, 1232 (1981).
[46] J. Mi and R. A. Antonia, Evolution of centreline temperature skewness in a circular cylinder wake, Int. Commun. Heat Mass Transf. **26**, 45 (1999).

[47] H. Rehab, R. A. Antonia, and L. Djenidi, Streamwise evolution of a high-schmidt-number passive scalar in a turbulent plane wake, Exp. Fluids **31**, 186 (2001).
[48] J. Mi, Y. Zhou, and G. J. Nathan, The effect of reynolds number on the passive scalar field in the turbulent wake of a circular cylinder, Flow, Turbul. Combust. **72**, 311 (2004).
[49] A. D. Pierce, Statistical theory of atmospheric turbulence effects on sonic-boom rise times, J. Acoust. Soc. Am. **49**, 906 (1971).
[50] K. Tanaka, T. Watanabe, and K. Nagata, Statistical analysis of deformation of a shock wave propagating in a local turbulent region, Phys. Fluids **32**, 096107 (2020).
[51] A. Sasoh, J.-H. Kim, and T. Sakai, Supersonic aerodynamic performance of truncated cones with repetitive laser pulse energy depositions, Shock Waves **24**, 59 (2014).